An Advanced Field Prediction Model Including Diffuse Scattering

Vittorio Degli-Esposti, *Member, IEEE*, Doriana Guiducci, Andrea de' Marsi, Pierfrancesco Azzi, and Franco Fuschini

***Abstract*—Ray tracing (RT) models are now widely adopted for field prediction in urban environment. Nevertheless, conventional RT tools still suffer for excessive central processing unit (CPU) time and inaccuracy in wide-band prediction. By increasing the maximum number of successive interactions (reflections, diffractions) little improvement in wide-band results can be usually achieved while CPU time increases exponentially. In the present paper, it is shown that by integrating reflection/diffraction with diffuse scattering, good narrow-band and wide-band results can be obtained with a low number of interactions. The adopted scattering model is a simple ray-based model, which has been embedded in a three-dimensional (3-D) RT program. The impact of diffuse scattering on narrowband and wide-band parameters is analyzed in the paper and the complete model is compared with measurements in a variety of cases, showing the validity of the approach.**

***Index Terms*—Land mobile radio, radio propagation, ray tracing, scattering, urban areas.**

I. Introduction

RADIO propagation in urban and suburban environment is a complex, multipath phenomenon which involves several different mechanisms. According to a traditional, simplified approach, two major urban propagation mechanisms are identified: over-roof-top (ORT) or vertical propagation (VP), where one major radial path undergoes multiple diffractions on building tops, and lateral propagation (LP), where several rays reflect/diffract on vertical building walls/edges according to the geometrical optics (GO) rules before reaching the receiver [1]. Several field prediction tools have been developed for the two categories: in particular, multiscreen diffraction models for VP [2] and two-dimensional (2-D) ray tracing (RT) models for the simulation of LP [1], [3], [4]. Unfortunately, in the common case of base station (BS) located at, or above, rooftops, VP and LP are not clearly definable. In such conditions 2-D-RT, multiscreen models or even a combination of them, often do not yield very good results, especially when wide-band estimates are needed. In fact, wide-band results are strongly affected by the presence of long-delay, oblique paths back-scattered by far objects such as building tops, tall buildings, hills, etc., which do not belong to the vertical nor to the lateral plane. These contributions often cannot be classified as reflections or diffractions but only as "diffuse scattering." Due to rough surfaces, decorative masonry, pipes, cables, internal irregularities, buildings often scatter energy in a wide range of directions apparently without following the GO rules. The corresponding contribution to the total field, although little, can have a significant impact on the "tail" of the power delay profile of the radio link. Some diffuse scattering models for urban radio propagation have been proposed in previous work [1]. Such models however are based on the Kirkhhoff approximation, which only takes into account surface roughness deviations with Gaussian statistics and a limited curvature. Therefore, this approximation is not very suitable for real building walls.

In the present work, a full three-dimensional (3-D) RT model has been developed and tested against wide-band measurements in typical urban environments. The developed model, beside deterministic reflection/diffraction, also takes into account scattering from building walls in a mean, statistical way according to the effective roughness (ER) model [5], [6].

After a description of the diffuse scattering model and of the RT program (Sections II and III), the impact of diffuse scattering on field prediction and more generally on propagation in various urban environments is analyzed in Section IV-A. Comparisons with measurements reported in Sections IV-B and IV-C show that good wide-band predictions can be obtained with a low number of interactions and thus with a relatively low computation time.

II. Modeling of Diffuse Scattering

When a radio wave impinges on a building wall, the field is scattered in a wide range of directions. If the wall is smooth and homogeneous, under the GO asymptotic hypotheses basic interaction mechanisms (reflections, diffractions) can be singled out. Unfortunately, real building walls are far from being smooth, homogeneous layers, and the problem is therefore a rather difficult one. The irregularities (windows, balconies, decorative masonry, rain-pipes, internal reinforcements, power lines, heating pipes, etc.) are usually comparable in size to the wavelength and no simple solution is available. Rigorous methods (finite elements, finite-difference time-domain, method of moments) are excessively time consuming, while asymptotic methods (GO, physical optics, UTD, etc.) have difficulty in treating compound scatterers, which is a common case [7].

In addition, the modeling of scattering from buildings cannot be regarded as a deterministic problem. Irregularities are usually not reported in building data bases and often *a priori* unknown.

Manuscript received March 7, 2003; revised September 30, 2003.

V. D. Degli-Esposito and F. Fuschini are with the Department of Electronics Engineering and Information Systems (DEIS), University of Bologna, 1-40126 Bologna, Italy (e-mail: vdegliesposti@deis.unibo.it; ffuschini@deis.unibo.it).

D. Guiducci was with the Department of Electronics Engineering and Information Systems (DEIS), University of Bologna, 1-40126 Bologna, Italy. She is now with the Ugo Bordoni Foundation, 00142 Rome, Italy.

A. de' Marsi is with ALSTOM Transport, Bologna 40044, Italy.

P. Azzi is with Ova G. Bargellini & C. SpA, 40066 Pieve di Cento (BO), Italy.

Digital Object Identifier 10.1109/TAP.2004.831299

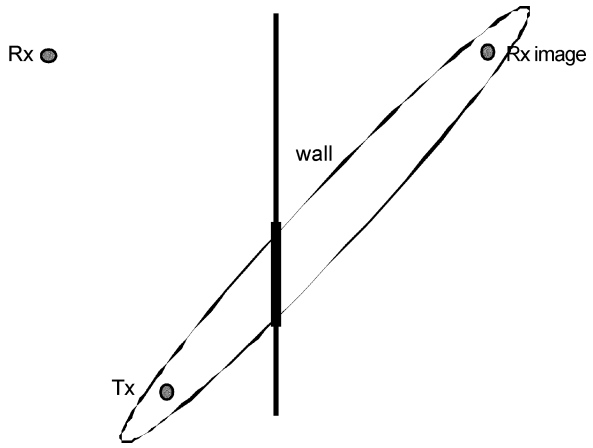

Fig. 1. Two radio terminals, a "close" wall and a Fresnel ellipsoid: the intersection between the wall and the ellipsoid is the "active" region of the wall for specular reflection.

Only the general characteristics of the building and of the expected irregularities are known and thus a statistical or hybrid approach should be adopted.

Several approaches to surface scattering are reported in the literature [8]–[10] and references therein. However, most of them are limited to Gaussian roughness and/or to small surface deviations with respect to the wavelength or small surface slope with respect to a flat surface, and this is not a common case for building walls.

In this paper, the new ER approach [5], [6] is adopted. Diffuse scattering is assumed originating from the surface of the building walls. A sort of ER is associated with each wall which takes into account not only real surface roughness but also the above mentioned surface/volume irregularities. The scattering contribution of each wall is computed directly from wall distance and orientation with respect to the Tx and the Rx using simple, analytic formulas which depend on only one parameter, the scattering parameter (S).

For simplicity, only first-order scattering is considered in the following. Extension to multiple scattering is straightforward. The model is used in a different way depending on the relative position of the considered wall with respect to the radio terminals.

A. Diffuse Scattering From "Close" Walls

When the wall is "close" to the radio terminals, i.e., when the first two or three Fresnel's ellipsoids, whose focuses are the Tx and the image of the Rx with respect to the wall, are fully intersected by the wall (see Fig. 1), the reflection contribution can be assumed equal to the specular reflection from an infinite surface and is therefore dominant [8]. Thus, the ER contribution is computed for "close" walls only when the direct reflected path is not present (when, for example, it is obstructed).

If a ray tube of aperture $d\Omega$ impinging on the generic surface element of the wall is now considered (see Fig. 2), part of the power is reflected in the specular ray tube, also of aperture $d\Omega$, part (P_P) is transmitted and part (P_S) is scattered in the upper half space. Each surface element is assumed to produce a noncoherent, Lambertian spherical scattered wave whose amplitude is $E_S = E_{S0}\sqrt{\cos(\theta_S)}$. The scattering coefficient S is defined as the ratio between the amplitude of the scattered field and the amplitude of the incident field in the vicinity of the surface. By expressing the power flowing through the tube as the product of the power density and the cross section of the tube and performing a simple power balance, the scattered field contribution at the receiving point can be obtained [5]

$$dE_S^2 = K_0^2 S^2 \frac{dS\cos\theta_i\cos\theta_S}{\pi}\frac{1}{r_i^2 r_S^2}; \quad K_0 = \sqrt{60 G_t P_t} \quad (1)$$

where G_t and P_t are the gain and the input power of the Tx antenna, respectively.

The value of the total scattered field can be calculated by integrating expression (1) over the wall surface. In order for the overall power balance to be satisfied, specular reflection and diffraction are consequently attenuated according to the Rayleigh factor R. Realistic, albeit probably diminutive, S and R values for typical buildings have been found to be $S = 0.4$ and $R = 0.6$ [5].

B. Diffuse Scattering From "Far" Walls

When the wall is "far" from the radio terminals, i.e., when the second or third Fresnel's ellipsoid are only partially intersected by the wall, or not intersected at all, we adopt a simplified version of the ER approach. Since the scattering angle (θ_s in Fig. 2) is now almost the same for all surface elements, the integral of expression (1) can be replaced by the following expression:

$$E_{S(\mathrm{TOT})}^2 = K_o^2 S^2 \frac{A\cos\theta_i\cos\theta_s}{\pi}\frac{1}{r_i^2 r_s^2} \quad (2)$$

where A is the surface area of the wall. This simplified approach corresponds to assuming a Lambertian scattering pattern for the entire "far" wall surface. The scattered ray is supposed springing from the barycentre of the wall.

Lambertian pattern may be considered not very realistic if regarded from a deterministic point of view. However, Lambertian scattering pattern yielded good results in recent work [5], [6]. Moreover, due to the great distance between the scatterer and the Rx and to the presence of peaks in realistic scattering patterns [11], even a small uncertainty in wall geometry or orientation may cause a great uncertainty in the signal level at the Rx. Therefore an average, Lambertian pattern, is likely to yield better results then a deterministic pattern.

Since scattered rays do not belong to the vertical plane nor to the horizontal plane adopted in traditional 2-D or 2-D+ 2-D approaches [1], [3], a fully 3-D approach must be adopted to properly model scattering phenomena in urban environment.

III. Prediction Model

The developed propagation prediction tool is based on an image RT technique combined with ER scattering. Buildings are modeled as right polygonal prisms of different heights. Terrain height is also taken into account.

According to the ray approach the radio signal at the Rx can be modeled as a set of rays. Each ray is associated with a complex, vectorial amplitude $\mathbf{E}_i$ which is computed according to the interactions (reflection, diffraction, scattering) experienced by the ray along its propagation path. The correct distance-decay

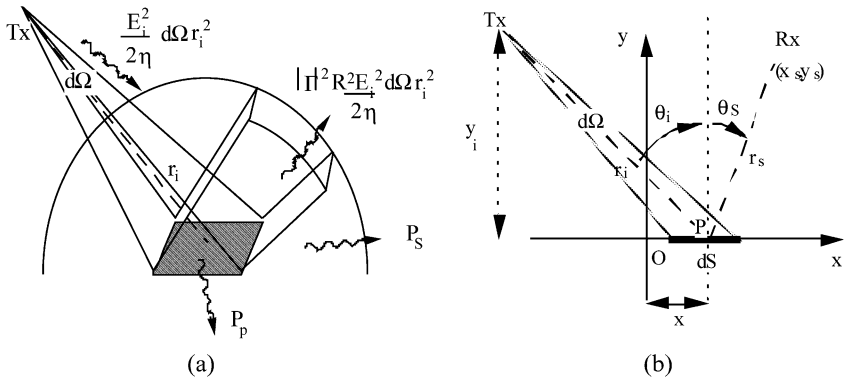

Fig. 2. (a) View of the generic surface element with the different power flows and (b) 2-D view in the xy plane with the surface element dS located at a distance x from the reflection point .

law (divergence factor) must be applied for the different propagation mechanisms (see [12] for diffracted rays and (2) for diffuse scattering). In particular, since the diffuse field decays with the product of the distances of the radio terminals from the scatterer, diffuse scattering plays an important role only if it occurs at the beginning or at the end of the interaction sequence.

The computation of the total field at the Rx point as a function of the field at a reference distance of 1 m from the Tx (in the direction of the ith ray), $\mathbf{E}_i(Tx)$, can be summarized with the following synthetic formula:

$$\mathbf{E}(Rx) = \sum_{i=o}^{N_r} \mathbf{E}_i(Rx) = \sum_{i=o}^{N_r} \left\{ \prod_{j=o}^{N_{\text{ev}}} \left[F^{\chi(i,j)} \mathbf{A}^{\chi(i,j)} P(i,j) \right] \mathbf{E}_i(Tx) \right\} \quad (3)$$

where N_r is the number of rays, N_{ev} is the maximum number of successive interactions considered by the model (see Section III-A), χ represents the kind of interaction, that is, either reflection, diffraction, scattering or ORT multiple diffraction (see Section III-B), $P(i,j)$ represents the spatial point where the jth interaction is assumed to take place, $\mathbf{A}$ is an appropriate dyadic to decompose the field into orthogonal components at the point $P(i,j)$ and includes the proper attenuation coefficients (reflection coefficients, diffraction coefficients, etc.). Finally $F^{\chi(i,j)}$ represents the *divergence factor* of interaction $\chi(i,j)$. Notice that, since not all rays experience the maximum number of interactions, we conventionally assume that several couples (i,j) correspond to a null divergence factor $F^{\chi(i,j)}$.

Since diffuse scattering must be considered incoherent, we either attribute a random phase and a random polarization to all rays experiencing at least one diffuse scattering interaction (incoherent rays), or we perform an incoherent power sum of all ray contributions. In this last case, the square amplitude of the electric field, instead of the complex, vectorial amplitude of it, should appear in (3). Results shown in Section IV have been obtained with the latter approach.

Similarly to previous work [3], the implemented RT algorithm consists of two main steps: the *visibility algorithm* and the *backtracking procedure*, as explained in the following subsections.

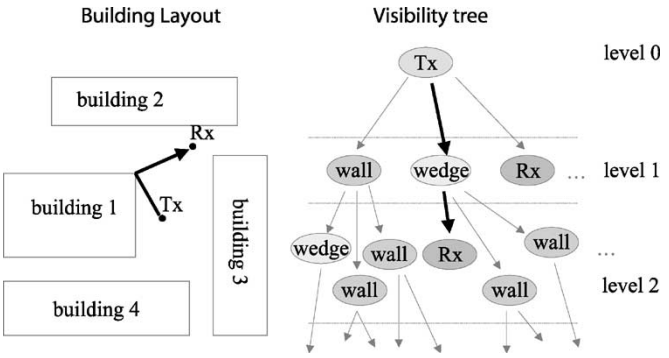

Fig. 3. Example of building layout and corresponding visibility tree.

A. Visibility Algorithm

The leading task of the visibility algorithm is the creation of the *visibility tree*, which is the core of the RT simulator. The visibility tree consists of nodes and branches and has a layered structure. Each node of the tree structure represents an *object* of the scenario, i.e., a building wall (or part of it), a wedge or the Rx terminal, whereas each branch represents a line-of-sight (LOS) visibility relation between two nodes (see Fig. 3).

Notice that the visibility relations among different nodes strongly depends on the considered propagation mechanisms. For example, a given object which is visible through diffuse scattering, may not be visible through reflection.

Starting from the root of the tree, which contains the Tx, the visibility tree is recursively built: nodes in the first layer contain all the objects that can be *seen* directly from the transmitter; similarly, second layer nodes contain the objects that can be *seen* from each first layer node. This procedure is repeated until the maximum allowed depth is reached. The maximum depth also corresponds to the maximum number of successive events (reflections, diffractions, scatterings, etc.) a ray can experience, N_{ev}. When a Rx is found a "leaf," an exit of the tree is created.

As far as diffraction visibility is considered, objects visible from a given wedge (i.e., visible from a point belonging to the wedge) are considered while building the visibility tree, regardless of the actual visibility through the Keller's cone [12]. The actual diffraction path is determined during the back-tracking phase, when visibility relations through diffraction which do not satisfy the Keller cone's constraints are discarded.

The creation of the visibility tree may require a great amount of central processing unit (CPU) time, especially in a full 3-D case and if $N_{\rm ev}$ is large. Therefore, an efficient visibility algorithm is essential.

According to the Image RT method, each node of the visibility tree is associated a virtual Tx [3]. Whenever a node is processed, the spherical reference system (ρ, θ, ϕ) centred in the virtual Tx is adopted. In order to determine the existing visibility relations while reducing CPU time with respect to traditional algorithms, the 3-D problem is transformed into two 2-D problems:

a) processing of the objects of the scenario in the (ρ, ϕ) plane (sweep line algorithm [13] and [14])
b) solution of the superposition of objects in (θ, ϕ).

In the (ρ, ϕ) plane walls and wedges are properly represented as *curved polar segments* and points lying on wall-edges respectively. A curved polar segment is defined by

$$\left[\left(\rho_n^i, \phi_n^i\right); \left(\rho_n^e, \phi_n^e\right); (\mathcal{A}, \mathcal{B})\right] \tag{4}$$

where (ρ_n^i, ϕ_n^i) and (ρ_n^e, ϕ_n^e) identify the extremes of the nth segment and $(\mathcal{A}, \mathcal{B})$ represent the degrees of freedom of a line in a plane. In the present paper, curved segments are approximated with polygonal lines: doing so, standard polygon clipping libraries can be used.

After having mapped the urban environment in the (ρ, ϕ) plane, a ϕ-sorted list is built, which contains the begin and end extremes of each segment. This list is then processed according to the sweep line algorithm [13], [14] in order to obtain a nonambiguous ρ-sorted list (the gray-box list in Fig. 4) where each wall either partially hides a successive wall or has no relation with it, i.e., the two walls are disjointed when seen from the actual point of view. The algorithm sweeps the environment with respect to ϕ with a vertical line, and sorts the walls having "order relations" with respect to ρ.

In the following step, all the elements in the ρ-sorted list are virtually drawn in the (θ, ϕ) plane as polygons [15]. Using the information in the ρ-sorted list, objects that are totally or partially visible from a virtual Tx are simply determined with consecutive polygon area subtractions so that the visible part of the nth object is expressed as

$$(\mathcal{ARE A})^n_{vis} = (\mathcal{ARE A})^n - \bigcup_{k<n} (\mathcal{ARE A})^k. \tag{5}$$

Whenever a visible object is identified, a node in the visibility tree is filled and the visibility algorithm processes recursively each new node.

Fig. 5 is obtained from a real urban scenario in the city of Stockholm and shows an example of visibility from a transmitter placed at the rooftop level. It is evident that in such a typical urban cell configuration a 2-D visibility algorithm would be inadequate.

B. Backtracking Procedure

Once the visibility tree is built, the backtracking procedure traces the optical rays starting from each leaf of the tree and heading up toward the root. It has to be reminded that each branch of the tree is associated a propagation mechanism, and

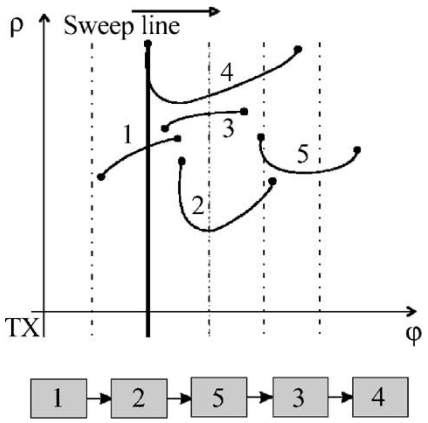

Fig. 4. Polar segments in the ρ, ϕ plane and the corresponding sweep-line algorithm output list.

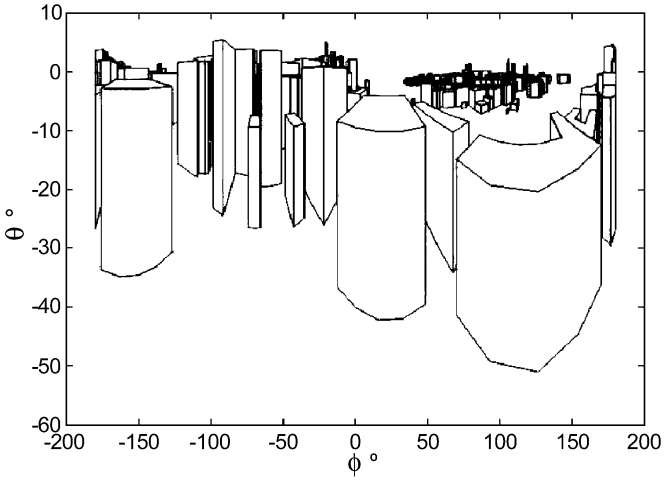

Fig. 5. View of Stockholm in the ρ, ϕ plane from a rooftop location.

the computation of the associated power loss strictly depends on it. Each time a reflection occurs, the Fresnel's reflection coefficients, multiplied by the Rayleigh coefficient R, are applied [8], [16]. When diffuse scattering occurs, the scattered field is computed as a function of the impinging wave field according to (1) or (2). When diffraction occurs on a building wedge, the procedure is different depending on wedge orientation, as explained in the following.

Diffraction From Vertical and Horizontal Edges: Since buildings are modeled as right polygonal prisms, two classes of edges can be identified, vertical (corner) edges and horizontal (rooftop) edges.

In the developed model, for efficiency reasons, diffraction around corners and ORT diffraction are evaluated in different ways. Diffraction from vertical edges is treated as the other interaction mechanisms within the 3-D algorithm. Each time a corner diffraction occurs, the field is multiplied by the proper UTD diffraction coefficients [12]. In the present paper, the simple perfectly conducting wedge coefficients multiplied by R are used. However, an extension to finite conductivity wedges is straightforward [17]. Notice that our approach may yield incorrect results when more than one successive diffraction takes place, and especially when edge separation is small [18].

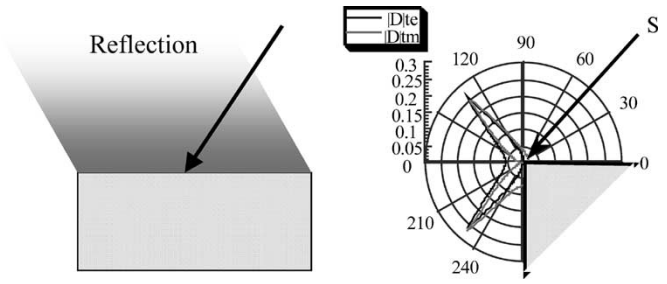

Fig. 6. Top view of a building illuminated by a far source. Reflection cone (left) and diffraction coefficients (for normal incidence) versus diffraction angle (right).

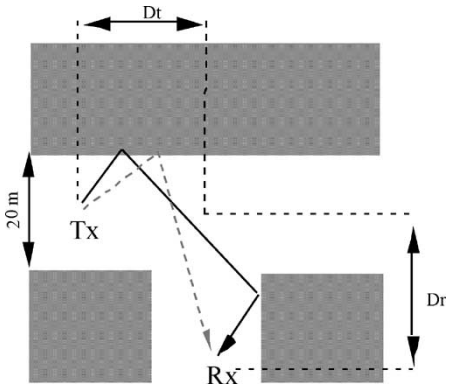

Fig. 7. T-shaped street intersection with a double-reflected ray (solid line) and a diffuse scattering ray (dashed line).

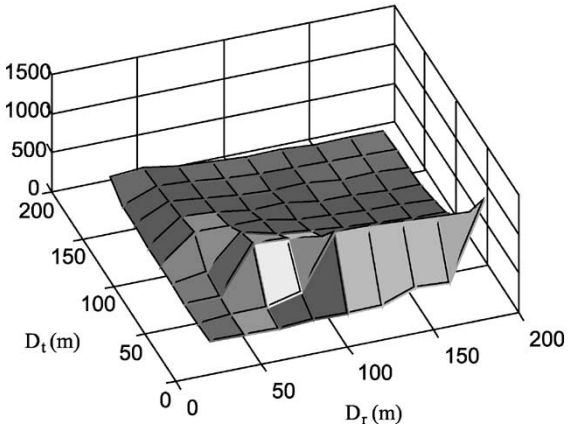

Fig. 8. Percent P_S ($P_S/P_{\rm GO}*100$) plotted against D_t and D_R (S = 0.316).

Alternative approaches have been developed which may permit to overcome this problem [19].

Diffraction from roof tops is treated in a different way. In a full 3-D view, ORT propagation is not limited to the shortest, radial ORT path, but any other path experiencing multiple bounces (reflection, scattering, etc.) on tall buildings and crossing the city over the roof tops before descending to street level should be considered. Therefore, a rigorous 3-D modeling of ORT propagation may require an overwhelming amount of computational resources. In order to lower CPU time requirements, ORT diffraction is de-embedded from the 3-D algorithm, and treated with an ad-hoc, simplified algorithm (see the last paragraph of this section). Horizontal edges are forced to be *invisible* in the 3-D core and therefore excluded from the visibility algorithm. Once the Visibility tree is built up, all the objects directly visible from at least one radio terminal are listed, and considered for ORT propagation. Based on this list, all rays experiencing one interaction with one of the listed objects and one ORT multidiffraction are traced. For example, all rays scattered from tall buildings (directly illuminated by the BS) and ORT-propagating before descending to the mobile are considered. Similarly, all rays experiencing ORT propagation and then descending to the mobile after one reflection or one scattering are traced. In other words, not only ORT on the vertical plane is taken into account, but VPs are traced also on the planes connecting virtual terminals corresponding to reflections or scatterings.

In order to evaluate ORT propagation, the simulated scenario is sliced with a vertical plane containing Tx and Rx (or a virtual image of one of the two), so that a 2-D scenario is obtained. Each obstacle is then represented with a knife edge and all superfluous edges are eliminated by using the "tight rope" method. Then an ad-hoc algorithm is used to compute ORT diffraction. For efficiency reasons we use the simple Epstein–Peterson method [20]. However, more sophisticated algorithms (e.g., [2] and [21]) can be used as well.

IV. Results

A. Analysis of the Impact of Diffuse Scattering

According to the GO theory, specular reflection and edge diffraction are only present in the reflection cone and on the Keller's cone, respectively. On the Keller's cone, diffraction is comparable in strength to the direct or reflected wave only on narrow peaks around the shadow boundaries (see Fig. 6), i.e., on the borders of the reflection cone or of the LOS region. Therefore, the coherent component (reflection/diffraction) does not represent a very efficient diffusion mechanisms because it is limited to a small subset of directions.

On the other hand, if we admit that part of the power incident on a building wall is diffused in all direction according to a given pattern, a number of important consequences must be pointed out.

In microcellular environment, where propagation mainly takes place *around* rather than *over* buildings, diffuse scattering can represent an efficient mean for transferring power around a street corner. Previous investigations on a X-shaped street intersection [5] have shown that the ER contribution is comparable or greater than the coherent contribution when the distances of the radio terminals D_t and D_r from the intersection are located on a hyperbola-shaped region.

With an approach similar to [5], we consider now a T-shaped street intersection (Fig. 7). The following values of electrical permittivity and conductivity for the building walls have been chosen: $\varepsilon_r = 5, \sigma = 1.e-2$ S/m. It is evident that the ER contribution (with the same cautious value of $S = 0.316$) appears even more evident than in the X-intersection case. Especially when the Tx is close to the intersection (but not in LOS) the scattered power P_S is several times greater than the GO power, $P_{\rm GO}$ (Fig. 8).

In Fig. 9 the root-mean-square (rms) delay spread (DS) [see Appendix I] versus D_R is reported for D_T equal to 30, 110, and

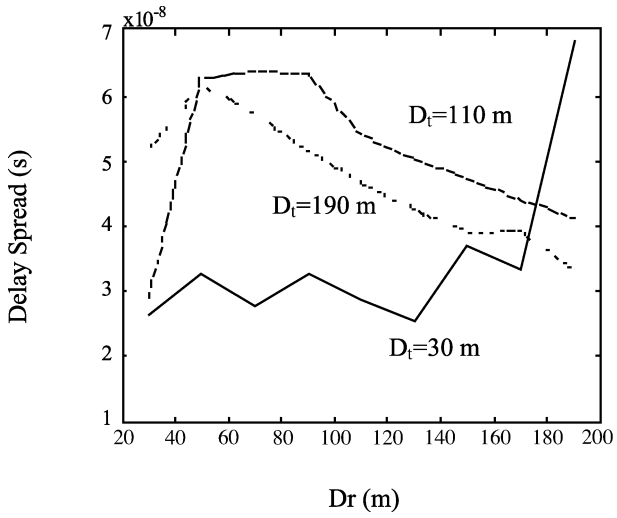

Fig. 9. DS versus D_R considering only the GO-contribution ($S = 0.316$).

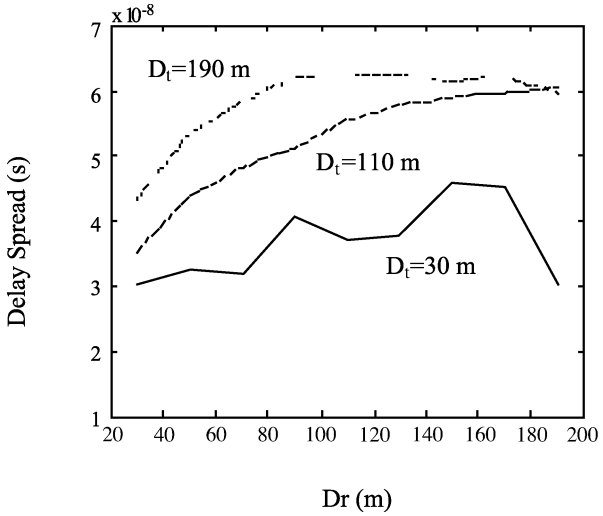

Fig. 10. DS versus D_R considering both the GO and the scattering contribution ($S = 0.316$).

190 m considering only the GO-contribution and with $N_{\text{ev}} = 6$. The corresponding results with both the GO and the scattering (ER) contributions is shown in Fig. 10. It is evident that the ER contribution has an important impact on both the absolute DS value and on its dependence on D_T and D_R. Notice that the shape of the curves is more uniform and realistic when scattering is included.

In macrocells, the impact of diffuse scattering is also very important. Due to the high location of the BS antenna with respect to the surrounding buildings, a dramatically higher number of buildings located over a wide area are directly illuminated by the BS. Therefore, a conspicuous number of rays can be down-scattered to the mobile from BS-illuminated buildings (in case, via an additional roof-to-street diffraction).

In this case, ER scattering can play a fundamental role. Let us consider for example a single, "far" wall and the radio terminals positioned as reported in Fig. 11. As usual, the cautious value $S = 0.4$ has been adopted and the coherent component has been consequently attenuated [5]. In Fig. 12 the back-scattering contribution for the coherent component (reflection+diffractions), for the incoherent ER scattering and for the combination of the two are shown. Since the ER model can be considered reliable, diffuse scattering must be considered very important or dominant if α is greater than 10–20°.

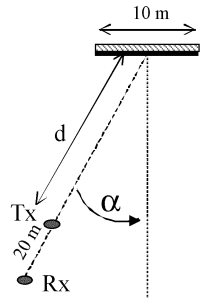

Fig. 11. Far wall and aligned Tx and Rx terminals; $d = 2$ km.

Thus, if we consider "far" buildings illuminated by a macrocellular BS, we can assert that:

1) excluding the reflection cone and surrounding directions, the coherent component is week compared to ER scattering;
2) rays [mainly scattered rays, because of 1)] are high-delay rays due to the great distance;
3) emission/arrival angles are spread over a wide range, and not only along streets or the radial Tx-Rx path.

Therefore, diffuse scattering has a major impact on both time- and angle-dispersion characteristics of the radio channel in small cells and macrocells. This is particularly relevant in future generation MIMO or smart antenna mobile radio systems.

B. Application to Microcellular Environment

The first results refer to a microcellular environment in the city of Fribourg, Switzerland, where SWISSCOM has performed a wide-band measurements campaign [4], [22]. Some measurement setup data are reported in Table I while the site is depicted in Fig. 13. RT prediction has been performed with the following parameters: $\varepsilon_{\text{r}} = 5$, $\sigma = 1.e-2$ [S/m], $N_{\text{ev}} = 5$. Here, the scattering parameter S has been set to 0.6 instead of 0.4 to take into account the effect of traffic and small objects (primarily lamp posts, which were present along the Rx street) which probably generated a great amount of back-scattering around the street intersection. In other words, we attributed to ER-scattering the effect of objects located not only "on" walls but also "next to" walls, such as lamp posts, and performed (only in this case) a sort of measurement-based tuning of S.

The improvement obtainable with diffuse scattering is evident from Figs. 14 and 15, where the field strength and the DS along the Rx route are reported. Notice that the DS agreement is not very good in the first part of the path: this is probably due to the presence of a path transmitted through the corner building, which is not included in the model. Transmission may have some relevance when a relatively small building section is interposed between the two radio terminals. The inclusion of transmission may therefore be of interest in microcells.

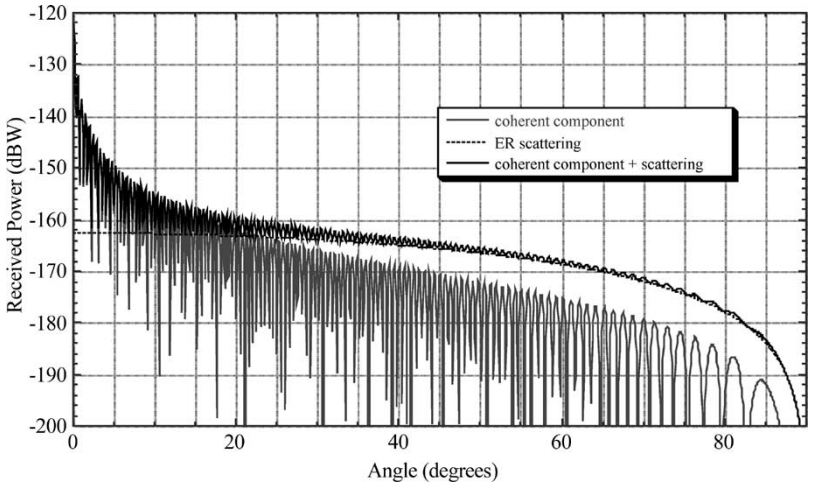

Fig. 12. Back-scattering from a metal, 10 × 10 m wall (see Fig. 11): reflection+diffraction (coherent component, gray line), ER scattering (dashed line) and combined (black line). ($P_t = 1\ W$, isotropic antennas, $S = 0.4$, $R = 0.9$).

TABLE I
FRIBOURG MEASUREMENTS DATA

The Fribourg measurements	
h_{TX} (m)	4
h_{RX} (m)	2
Frequency (MHz)	1800
Emitted power (W)	1
Path length (m)	112.5
Antenna types	Half wavelength dipoles

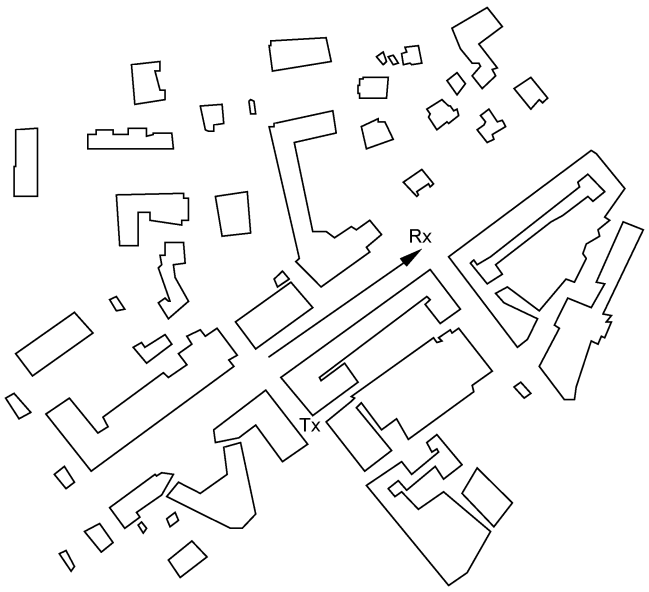

Fig. 13. Fribourg site.

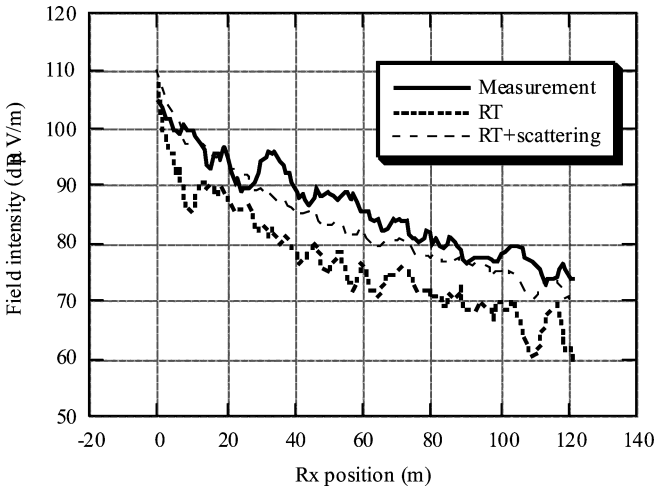

Fig. 14. Measured and RT-predicted field strength with and without the scattering contribution (Fribourg).

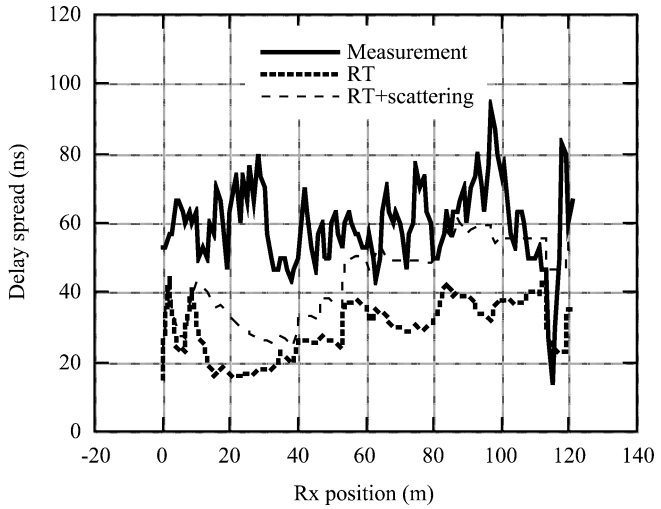

Fig. 15. Measured and RT-predicted rms DS with and without the scattering contribution (Fribourg).

C. Application to Macrocellular Environment

The developed 3-D RT tool has been applied to a macrocellular scenario in the city of Stockholm. The input scenario is a 2 × 2 km 3-D vectorial data base where buildings of similar height have been grouped into city blocks, for a total of about 500 walls (Fig. 16). Terrain height has also been considered. To the author's knowledge, this is the first time that 3-D wide-band prediction is carried out in a macrocellular case with good results. Since the Tx is placed above the mean roof-top level, and

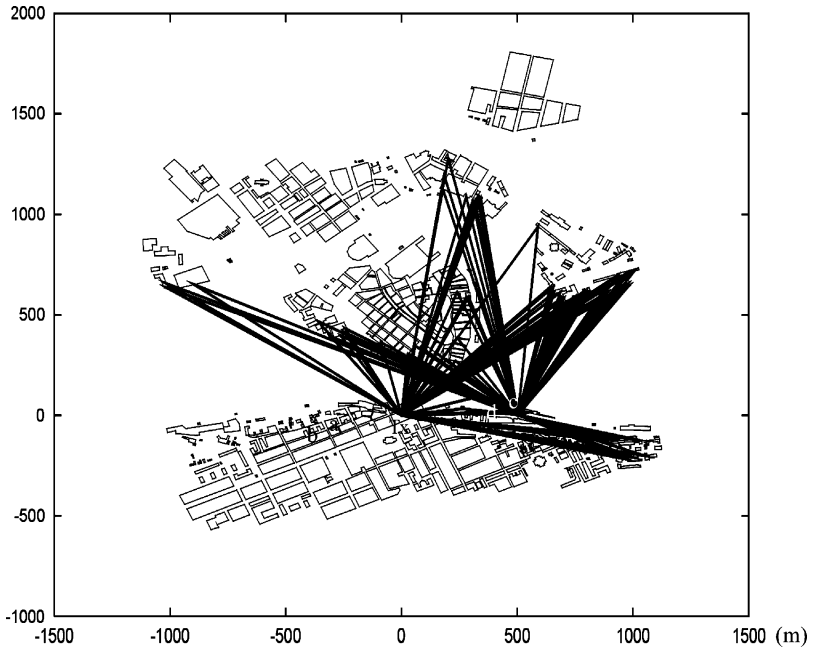

Fig. 16. Stockholm scenario with the Tx (base station), the considered Rx locations and some major scattered rays (Rx in location c).

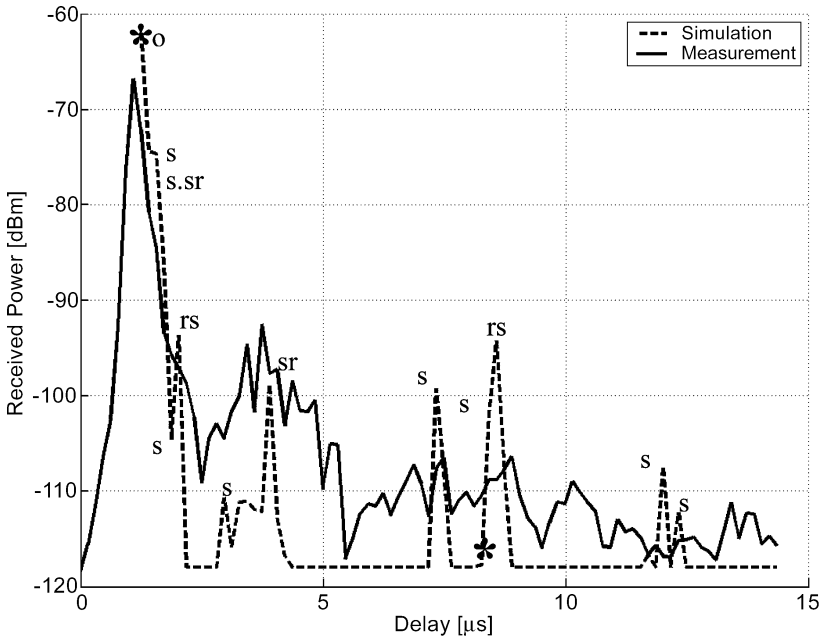

Fig. 17. Location "a": measured PDP (solid line) and predicted PDP (dashed line) with dominant mechanism tags. The asterisks represent the peaks of the PDP predicted with conventional GO-RT.

because of the particular morphological structure of the considered area, many far buildings are directly visible from both Tx and Rx. In such a configuration a considerable percentage of power reaches the Rx after being back-scattered by far objects. RT predictions have been performed with the following parameters: $\varepsilon_r = 8$, $\sigma = 1.e-3$ S/m, $S = 0.4$, $N_{\text{ev}} = 2$.

Figs. 17–20 report the measured and predicted power delay profiles (PDPs) corresponding to the Rx locations "a" to "d," respectively (Fig. 16). Measured PDPs are obtained with a sliding correlator channel sounder as illustrated in [23] and in references therein. Predicted PDPs are obtained dividing the time span into 156 ns bins and summing up for each time bin the power contributions of the paths falling into the bin. It is evident that the overall shape of the PDPs is well reproduced by the model. The propagation mechanisms corresponding to the dominant ray(s) are also shown in Figs. 17–20 with labels beside the corresponding peaks using the symbols listed in Table II. If the dominant ray undergo more than one interaction, more than one symbol is shown. For example, if the couple of symbols "so" is shown, the dominant ray experienced scattering and then ORT diffraction. If there is more than one dominant ray (within a power range of 3 dBs) a dot is interposed between the symbols. For legibility only the major peaks have been labeled.

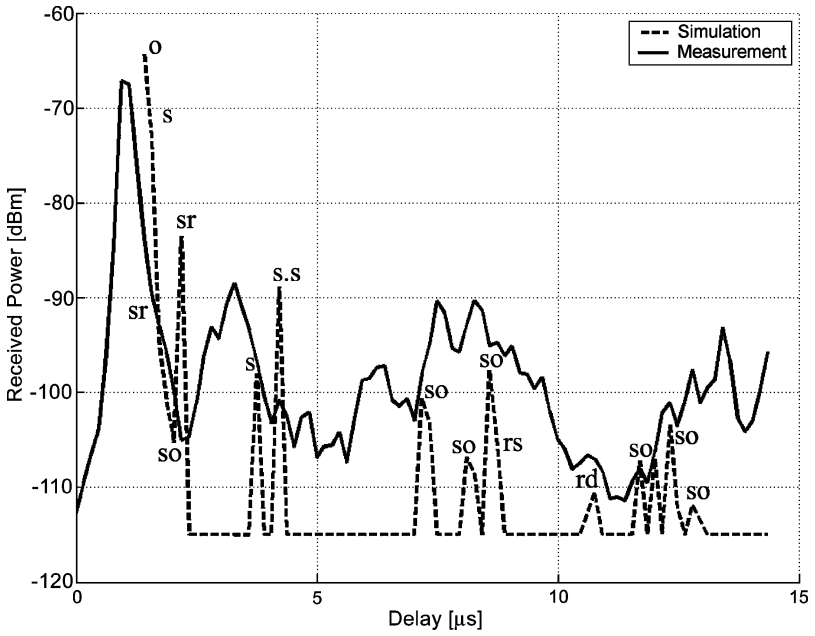

Fig. 18. Location "b": measured PDP (solid line) and predicted PDP (dashed line) with dominant mechanism tags.

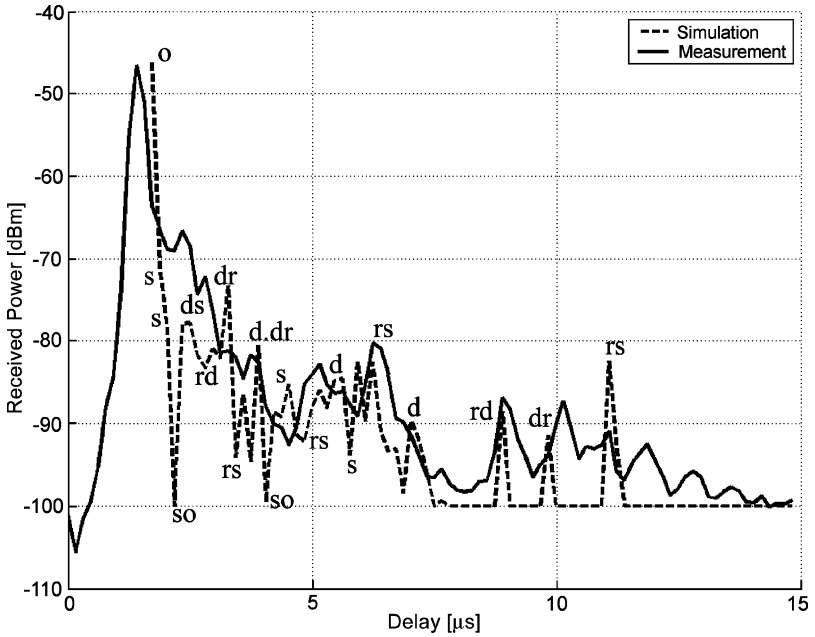

Fig. 19. Location "c": measured PDP (solid line) and predicted PDP (dashed line) with dominant mechanism tags.

TABLE II
SYMBOLS AND CORRESPONDING PROPAGATION MECHANISM

Symbol	Mechanisms
r	reflection
d	diffraction
s	scattering
o	ORT (multi diffraction)

It must be noticed that diffuse scattering is probably the most relevant propagation mechanism: beside the first peak, which is obviously due to LOS or ORT, scattering is involved in almost all the remaining peaks. Scattering combined with ORT ("so") appears to be the most important mechanism in locations a and b, while scattering or diffraction combined with reflection is also important in location "c." This is probably due to the fact that locations a,b (and partially d) are "sunken" into the urban structure, while location c faces an open water basin. In Fig. 17 the PDP predicted with conventional RT is also represented with two asterisks: it is evident that conventional GO-RT, which only predicts one single path beside the main one, is not able to reproduce acceptable PDPs with the same number of events, N_{ev}.

Measurements and predictions have also been compared in terms of DS (see Appendix I) and path loss (PL). The results are reported in Table III.

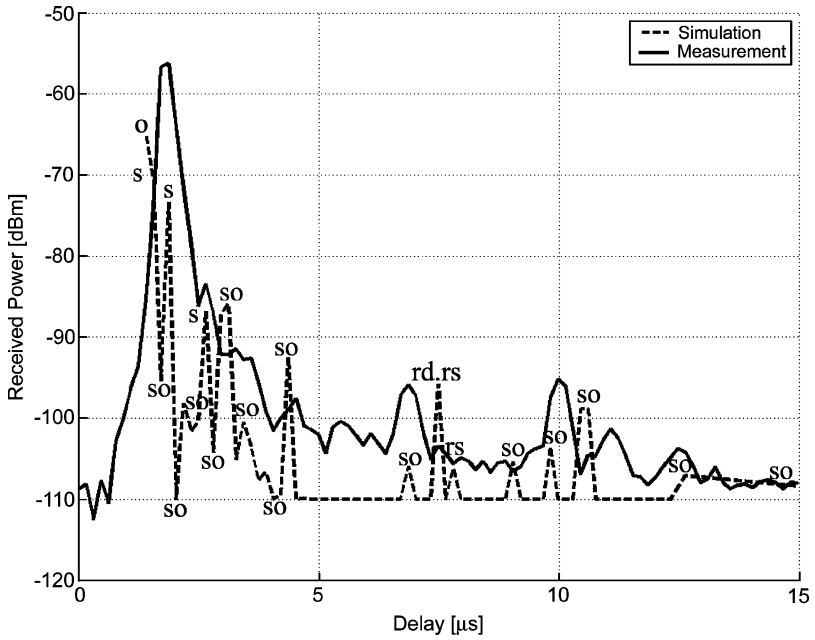

Fig. 20. Location "d": measured PDP (solid line) and predicted PDP (dashed line) with dominant mechanism tags.

TABLE III
COMPARISON BETWEEN MEASURED AND PREDICTED PATH LOSS (PL) AND DELAY SPREAD (DS)

Location	Measured PL (dB)	Predicted PL (dB)	Measured DS (μs)	Predicted DS (μs)
a	65	61	0.41	0.23
b	64	63	1.5	0.31
c	45	46	0.34	0.24
d	55	63	0.27	0.39

It is interesting to observe that the disagreements in Table III are always associated with errors in the main peak value (see Figs. 17–20), even when this peak corresponds to LOS propagation. The DS is underestimated in locations a and b (the PL is slightly overestimated) where the peak is overestimated, while the PL is overestimated in location d (the DS is slightly underestimated) where the peak is underestimated.

Also, the time alignment of the main peak is not always good. Since errors in the main peak are probably due to inaccuracies in the data base (inaccuracies either in the building data or in the terminal locations), we must conclude that data base accuracy has a strong influence on prediction results, and that further refinements can only be achieved with accurate input data.

While the computation time is negligible in the smaller environments considered in Sections IV-A and IV-B, it is of the order of hours (on standard, 2 GHz PC/Linux computers) in the Stockholm case due to the much larger number of buildings involved in the propagation process, i.e., the much larger number of walls visible from the BS. Therefore, speed-up techniques such as the *bounding boxes technique* [24] and others [25] are of major importance and will have to be considered in further developments.

V. CONCLUSION

A novel 3-D RT model which is partly based on GO/UTD and partly on the ER approach for the evaluation of diffuse scattering, has been presented. The diffuse component has been shown to be of major importance, especially for wide-band assessments in macrocells. The model has been checked against measurements in a variety of cases and good narrow-band and wide-band results have been obtained with a low number of interactions. Even in difficult cases, such as wide-band prediction in macrocells, where usually traditional RT tools do not yield realistic prediction, the model gives acceptable results. The prediction accuracy however, is largely bounded by the accuracy of the database.

APPENDIX I
RMS DELAY SPREAD AND ITS COMPUTATION

In the present paper, the rms DS is computed as follows:

$$\mathrm{DS} = \sqrt{\frac{\sum_{\mathrm{i}} \mathrm{p_i}(\xi_{\mathrm{i}} - \xi_{\mathrm{M}})^2}{\sum_{\mathrm{i}} \mathrm{p_i}}}$$

where ξ_i represent the excess delay, i.e., the delay with respect to the first peak at the Rx, and p_i the power level contribution of the ith path, whereas xi_M is the mean excess delay of all the paths at the Rx, which can be computed as

$$xi_M = \sqrt{\frac{\sum_i p_i xi_i}{\sum_i p_i}}.$$

In order to evaluate the DS in the urban scenario of Stockholm, only peaks within a cutoff threshold of about 50 dB with respect to the strongest peak, have been taken into account. The precise threshold value depends on the particular measurement and corresponds to the measurement noise floor.

ACKNOWLEDGMENT

The authors would like to thank ERICSSON and SWISSCOM for having provided them with the measurements used in this paper.

REFERENCES

[1] T. Kurner, D. J. Cichon, and W. Wiesbeck, "Concepts and results for 3D digital terrain-based wave propagation models: An overview," *IEEE J. Select. Areas Commun.*, vol. 11, pp. 1002–1012, 1993.

[2] J. Walfish and H. L. Bertoni, "A theoretical model of UHF propagation in urban environments," *IEEE Trans. Antennas Propagat.*, vol. 36, pp. 1788–1796, Dec. 1998.

[3] P. Daniele, V. D. Esposti, G. Falciasecca, and G. Riva, "Field prediction tools for wireless communications in outdoor and indoor environments," in *Proc. IEEE MTT-S Eur. Topical Congr. Technologies for Wireless Applications*, Turin, Italy, Nov. 2–4, 1994, pp. 129–134.

[4] K. Rizk, J.-F. Wagen, and F. Gardiol, "Two dimensional ray tracing modeling for propagation prediction in microcellular environments," *IEEE Trans. Veh. Technol.*, vol. 46, pp. 508–518, May 1997.

[5] V. Degli-Esposti and H. L. Bertoni, "Evaluation of the role of diffuse scattering in urban microcellular propagation," in *Proc. IEEE-VTC'99—Fall*, Amsterdam, The Netherlands, Sept. 19–22, 1999.

[6] V. D. Esposti, "A diffuse scattering model for urban propagation prediction," *IEEE Trans. Antennas Propagat.*, vol. 49, pp. 1111–1113, July 2001.

[7] P.-P. Borsboom and A. Zebic-Le Hyaric, "RCS predictions using wide-angle PE codes," in *Proc. 10th Int. Conf. Antennas and Propagation*, 1997, no. 436, pp. 2.191–2.194.

[8] P. Beckmann and A. Spizzichino, *The Scattering of Electromagnetic Waves From Rough Surfaces*. Oxford, U.K.: Pergamon Press, 1963.

[9] S. K. Nayar, K. Ikeuchi, and T. Kanade, "Surface reflection: physical and geometrical perspectives," *IEEE Trans. Pattern Analysis Machine Intelligence*, vol. 13, July 1991.

[10] I. M. Fuks, "Wave diffraction by a rough boundary of an arbitrary plane-layered medium," *IEEE Trans. Antennas Propagat.*, vol. 49, pp. 630–639, Apr. 2001.

[11] M. O. Al-Nuaimi and M. S. Ding, "Prediction models and measurements of microwave signals scattered from buildings," *IEEE Trans. Antennas Propagat.*, vol. 42, pp. 1126–1137, Aug. 1994.

[12] R. G. Kouyoumjian and P. H. Pathak, "A uniform geometrical theory of diffraction for an edge in a perfectly conducting surface," *Proc. IEEE*, vol. 62, pp. 1448–1461, Nov. 1974.

[13] J. Maurer, O. Drumm, D. Didascalou, and W. Wiesbeck, "A novel approach in the determination of visible surfaces in 3D vector geometries for Ray-Optical wave propagation modeling," in *Proc. Vehicular Technology Conf.*, vol. 3, Tokyo, 2000, pp. 1651–1655.

[14] M. de Berg, M. van Kreveld, M. Overmars, and O. Schwarzkopf, *Computational Geometry—Algorithms and Applications*. Berlin Heidelberg, Germany: Springer, 1997.

[15] M. F. Catedra, J. Perez, F. Saez de Adana, and O. Gutierrez, "Efficient ray-tracing techniques for three-dimensional analyzes of propagation in mobile communication: application to picocell and microcell scenarios," *IEEE Antennas Propagat. Mag.*, vol. 40, pp. 15–28, Apr. 1998.

[16] C. A. Balanis, *Advanced Engineering Electromagnetics*. New York: Wiley, 1989.

[17] R. J. Luebbers, "Finite conductivity uniform GTD versus knife edge diffraction in prediction of propagation path loss," *IEEE Trans. Antennas Propagat.*, vol. 32, pp. 70–76, Jan. 1984.

[18] D. Erricolo, "Experimental validation of second-order diffraction coefficients for computation of path-loss past buildings," *IEEE Trans. Electromagn. Compat.*, vol. 44, pp. 272–273, Feb. 2002.

[19] M. Albani, F. Capolino, S. Maci, and R. Tiberio, "Diffraction at a thick screen including corrugations on the top face," *IEEE Trans. Antennas Propagat.*, vol. 45, pp. 277–283, Feb. 1997.

[20] J. D. Parsons, *The Mobile Radio Propagation Channel*, 2nd ed. New York: Wiley, 2000.

[21] S. R. Saunders and F. R. Bonar, "Prediction of mobile radio wave propagation over buildings of irregular heights and spacings," *IEEE Trans. Antennas Propagat.*, vol. 42, pp. 137–144, Feb. 1994.

[22] K. Rizk, J. F. Wagen, and F. Gardiol, "Influence of database accuracy on two-dimensional ray-tracing-based prediction in urban microcells," *IEEE Trans. Veh. Technol.*, vol. 49, pp. 631–642, Mar. 2000.

[23] A. A. Glazunov, H. Asplund, and J.-E. Berg, "Statistical analysis of measured short-term impulse response functions of 1.88 GHz radio channels in Stockholm with corresponding channel model," in *Proc. IEEE-VTC'99—Fall*, Amsterdam, The Netherlands, Sept. 19–22, 1999.

[24] F. Aguado Agelet, A. Formella, J. M. Hernando Rabanos, F. Isasi de Vicente, and F. Perez Fontan, "Efficient ray tracing acceleration techniques for radio propagation modeling," *IEEE Trans. Veh. Technol.*, vol. 49, pp. 2089–2104, Nov. 2000.

[25] N. P. Wilt, *Object-Oriented Ray-Tracing in C++*. New York: Wiley, 1994.

Vittorio Degli-Esposti (M'94) received the Laurea degree (with honors) and the Ph.D. degree in electronic engineering from the University of Bologna, Bologna, Italy, in 1989 and in 1994, respectively.

From 1989 to 1990, he was with Siemens Telecomunicazioni, Milan, Italy, involved in research on high-speed optical fiber communication systems. Since November 1994, he has been with the Department of Electronics Engineering and Information Systems (DEIS), University of Bologna. In 1998, he was a Visiting Researcher at the Polytechnic University, Brooklyn, NY, working with Professor H. L. Bertoni on diffuse scattering models for urban propagation prediction. Since January 2000, he has been holding teaching appointments on radio propagation at the University of Bologna, where in April 2003, he received qualification as an Associate Professor. He participated in the European Cooperation Projects COST 231, COST 259, and COST 273. He is the author or coauthor of more than 50 technical papers in the fields of applied electromagnetics, radio propagation, and mobile radio systems. His current research interests are in the fields of mobile radio propagation, applied electromagnetics, diffuse scattering models, ray tracing and advanced statistical models for urban field prediction.

Dr. Degli-Esposti is a Member of the IEEE Antennas and Propagation Society. He serves as Reviewer for a number of international journals including IEEE TRANSACTIONS ON ANTENNAS AND PROPAGATION, IEEE JOURNAL ON SELECTED AREAS IN COMMUNICATIONS, IEEE COMMUNICATION LETTERS, IEEE TRANSACTIONS ON VEHICULAR TECHNOLOGY, and IEEE TRANSACTIONS ON WIRELESS COMMUNICATIONS.

Doriana Guiducci was born in Bologna, Italy, in 1974. She received the Laurea degree in telecommunications engineering and the Ph.D. degree in computer science and electronics engineering from the University of Bologna, in 1999 and 2003, respectively. In 2000, she attended a Master in radiocommunications engineering held by the University of Bologna.

She participated in the European Cooperation Action COST 273. She is currently working with the Ugo Bordoni Foundation, Rome, Italy, where she is involved in a national project for the deployment of an electromagnetic field monitoring network. Her research interests are on mobile communications and particularly on channel modeling.

Andrea de' Marsi received the Laurea degree in telecommunication engineering from the University of Bologna, Bologna, Italy, in 2001.

During 2001, he was a collaborator of the Department of Electronics Engineering and Information Systems (DEIS), University of Bologna, where he was involved in a research program on mobile radio propagation, diffuse scattering models, ray tracing and advanced statistical models for urban field prediction. He participated in the European Cooperation Projects COST 273. In 2002, he was with WAVECALL, Lausanne, Switzerland, working on ray tracing field prediction models. Currently, he is with ALSTOM Transport, Bologna.

Pierfrancesco Azzi received the Laurea degree in telecommunication engineering from the University of Bologna, Bologna, Italy, in 2001.

From 2001 to 2002, he was a collaborator of the Department of Electronics Engineering and Information Systems (DEIS), University of Bologna, and the Guglielmo Marconi Foundation, Bedford, NH. He participated in the European Cooperation Projects COST 273. He was involved in a research program on mobile radio propagation, diffuse scattering models, ray tracing and advanced statistical models for urban field prediction. He is currently with Ova G. Bargellini & C. SpA, Pieve di Cento, Italy

Franco Fuschini was born in Bologna, Italy, in 1973. He received the Laurea degree in telecommunication engineering and the Ph.D. degree in electronics and computer science from the University of Bologna in March 1999 and in July 2003, respectively.

He participated in the European Cooperation Project COST 273. He is now a Research Associate in the Department of Electronics Engineering and Information Systems (DEIS), University of Bologna. His research interests are in the field of mobile communications and particularly of statistical field prediction models and advanced ray tracing simulators for urban propagation.